Ultra-high quality factor optical resonators based on semiconductor nanowires

Yinan Zhang,[*] Marko Lončar

School of Engineering and Applied Sciences, Harvard University, 33 Oxford Street, Cambridge, MA 02138, USA
[*]Corresponding author: yinan@seas.harvard.edu

Abstract: We propose a platform to achieve ultra-high Quality factor (Q) optical resonators based on semiconductor nanowires. By defining one-dimensional photonic crystal at nanowire ends and engineering the micro-cavity pattern, cavities with Q of 3×10^5 and mode volume smaller than $0.2(\lambda/n)^3$ have been designed. This represents an increase of almost three orders of magnitude over the Quality factor of an as-grown nanowire. Our cavities are well-suited for the realization of nanowire-based low-threshold lasers, single-photon sources and quantum optical devices that operate in the strong-coupling limit.

OCIS codes: (230.5750) Resonators; (230.3990) Micro-optical devices; (270.0270) Quantum optics.

References and links

1. M. H. Huang, S. Mao, H. Feick, H. Yan, Y. Wu, H. Kind, E. Weber, R. Russo, and P. Yang, "Room-temperature ultraviolet nanowire nanolasers," Science **292**, 1897-1899 (2001).
2. X. Duan, Y. Huang, R. Agarwal, and C. M. Lieber, "Single-nanowire electrically driven laser," Nature **421**, 241-245 (2003).
3. R. Agarwal, C. J. Barrelet, and C. M. Lieber, "Lasing in single cadmium sulfide nanowire optical cavities," Nano. Lett. **5**, 917-920 (2005).
4. S. Gradecek, F. Qian, Y. Li, H. G. Park, and C. M. Lieber, "GaN nanowire lasers with low lasing threshold," Appl. Phys. Lett. **87**, 173111 (2005).
5. J. M. Bao, M. Zimmler, F. Capasso, X. Wang, and Z. F. Ren, "Broadband ZnO single-nanowire light-emitting diode," Nano. Lett. **6**, 1719-1722 (2006).
6. J. C. Johnson, H. Yan, P. Yang, and R. J. Saykally, "Optical cavity effects in ZnO nanowire lasers and waveguides," J. Phys. Chem. B **107**, 8816-8828 (2003).
7. A. V. Maslov and C. Z. Ning, "Reflection of guided modes in a semiconductor nanowire laser," Appl. Phys. Lett. **83**, 1237-1239 (2003).
8. Z. Y. Li and K. M. Ho, "Bloch mode reflection and lasing threshold in semiconductor nanowire laser arrays," Physical Review B **71**, 045315 (2005).
9. M. Q. Wang, Y. Z. Huang, Q. Chen, and Z. P. Cai, "Analysis of mode quality factors and mode reflectivities for nanowire cavity by FDTD technique," IEEE J. Quantum Electron. **42**, 146-151 (2006).
10. Y. Ding, J. Motohisa, B. Hua, S. Hara, and T. Fukui, "Observation of microcavity modes and waveguides in InP nanowires fabricated by selective-area metalorganic vapor-phase epitaxy," Nano. Lett. **7**, 3598-3602 (2007).
11. A. V. Maslov and C. Z. Ning, "Modal gain in a semiconductor nanowire laser with anisotropic bandstructure," IEEE J. Quantum Electron. **40**, 1389-1397 (2004).
12. C. Barrelet, J. Bao, M. Loncar, H. G. Park, F. Capasso, and C. M. Lieber, "Hybrid single-nanowire photonic crystal and microresonator structures," Nano. Lett. **6**, 11-15 (2006).
13. O. L. Muskens, J. Treffers, M. Forcales, M. T. Borgstrom, E. P. A. M. Bakkers, and J. G. Rivas, "Modification of the photoluminescence anisotropy of semiconductor nanowires by coupling to surface plasmon polaritons," Opt. Lett. **32**, 2097-2099 (2007).
14. H. G. Park, F. Qian, C. J. Barrelet, and Y. Li, "Microstadium single-nanowire laser," Appl. Phys. Lett. **91**, 251115 (2007).
15. M. Pelton, C. Santori, J. Vuckovic, B. Zhang, G. S. Solomon, J. Plant, and Y. Yamamoto, "Efficient source of single photons: A single quantum dot in a micropost microcavity," Phys. Rev. Lett. **89**, 233602 (2002).
16. P. Michler, A. Kiraz, C. Becher, W. V. Schoenfeld, P. M. Petroff, L. Zhang, E. Hu, and A. Imamoglu, "A quantum dot single-photon turnstile device," Science **290**, 2282-2285 (2000).

#100129 - $15.00 USD Received 13 Aug 2008; revised 18 Sep 2008; accepted 8 Oct 2008; published 15 Oct 2008

17. D. Englund, D. Fattal, E. Waks, G. Solomon, B. Zhang, T. Nakaoka, Y. Arakawa, Y. Yamamoto, and J. Vuckovic, "Controlling the spontaneous emission rate of single quantum dots in a two-dimensional photonic crystals," Phys. Rev. Lett. **95**, 013904 (2005).
18. M. S. Gudiksen, L. J. Lauhon, J. Wang, D. C. Smith, and C. M. Lieber, "Growth of nanowire superlattice structures for nanoscale photonics and electronics," Nature **415**, 617-620 (2002).
19. M. T. Bjork, B. J. Ohlsson, T. Sass, A. I. Persson, C. Thelander, M. H. Magnusson, K. Deppert, L. R. Wallenberg, and L. Samuelson, "One-dimensional heterostructures in semiconductor nanowhiskers," Appl. Phys. Lett. **80**, 1058-1060 (2002).
20. N. Panev, A. I. Persson, N. Skold, and L. Samuelson, "Sharp exciton emission from single InAs quantum dots in GaAs nanowires," Appl. Phys. Lett. **83**, 2238-2240 (2003).
21. L. Samuelson, M. T. Bjork, K. Deppert, M. Larsson, B. J. Ohlsson, N. Panev, A. I. Persson, N. Skold, C. Thelander, and L. R. Wallenberg, "Semiconductor nanowires for novel one-dimensional devices," Physica E **21**, 560-567 (2004).
22. M. T. Bjork, C. Thelander, A. E. Hansen, L. E. Jenson, M. W. Larsson, L. R. Wallenberg, and L. Samuelson, "Few-electron quantum dots in nanowires," Nano. Lett. **4**, 1621-1625 (2004).
23. C. P. T. Svensson, W. Seifert, M. W. Larsson, L. R. Wallenberg, J. Stangl, G. Bauer, and L. Samuelson, "Epitaxially grown GaP/ GaAs1-xPx/GaP double heterostructure nanowires for optical applications," Nanotechnology **16**, 936-939 (2005).
24. M. T. Borgstrom, V. Zwiller, E. Muller, and A. Imamoglu, "Optically bright quantum dots in single nanowires," Nano. Lett. **5**, 1439-1443 (2005).
25. E. D. Minot, F. Kelkensberg, M. v. Kouwen, J. A. v. Dam, L. P. Kouwenhoven, V. Zwiller, M. T. Borgstrom, O. Wunnicke, M. A. Verheijen, and E. P. A. M. Bakkers, "Single quantum dot nanowire LEDs," Nano. Lett. **7**, 367-371 (2007).
26. P. Lalanne and J. P. Hugonin, "Bloch-wave engineering for high-Q, small-V microcavities," IEEE J. Quantum Electron. **39**, 1430-1438 (2003).
27. H. J. Kimble, in *Cavity Electrodynamics*, P. Berman, ed. (Academic Press, San Diego, 1994).
28. A. Yariv, *Photonics: Optical electronics in modern communications*, 6 ed. (Oxford University Press, 2006).
29. L. Tong, J. Lou, and E. Mazur, "Single-mode guiding properties of subwavelength-diameter silica and silicon wire waveguides," Opt. Express **12**, 1025-1035 (2004).
30. M. Palamaru and P. Lalanne, "Photonic crystal waveguides: Out-of-plane losses and adiabatic modal conversion," Appl. Phys. Lett. **78**, 1466-1468 (2001).
31. C. Sauvan, G. Lecamp, P. Lalanne, and J. P. Hugonin, "Modal-reflectivity enhancement by geometry tuning in Photonic Crystal microcavities," Opt. Express **13**, 245-255 (2005).
32. P. Velha, E. Picard, T. Charvolin, E. Hadji, J. C. Rodier, P. Lalanne, and D. Peyrade, "Ultra-high Q/V Fabry-Perot microcavity on SOI substrate," Opt. Express **15**, 16090-16096 (2007).
33. A. I. Persson, M. T. Bjork, S. Jeppesen, J. B. Wagner, L. R. Wallenberg, and L. Samuelson, "InAs1-xPx nanowires for device engineering," Nano. Lett. **6**, 403-407 (2006).
34. S. K. Lim, M. J. Tambe, M. M. Brewster, and S. Gradecak, "Controlled growth of ternary alloy nanowires using metalorganic chemical vapor deposition," Nano. Lett. **8**, 1386-1392 (2008).
35. M. Notomi, E. Kuramochi, and H. Taniyama, "Ultrahigh-Q nanocavity with 1D photonic gap," Opt. Express **16**, 11095-11102 (2008).
36. T. Asano, B. S. Song, Y. Akahane, and S. Noda, "Ultrahigh-Q nanocavities in two-dimensional photonic crystal slabs," IEEE J. Sel. Top. Quantum Electron. **12**, 1123-1134 (2006).
37. B. S. Song, S. Noda, T. Asano, and Y. Akahane, "Ultra-high-Q photonic double-heterostructure nanocavity," Nat. Mater. **4**, 207-210 (2005).
38. Y. Tanaka, T. Asano, and S. Noda, "Design of photonic crystal nanocavity with Q-factor of similar to 10(9)," J. Lightwave Technol. **26**, 1532-1539 (2008).
39. D. Englund, I. Fushman, and J. Vuckovic, "General recipe for designing photonic crystal cavities," Opt. Express **13**, 5961-5975 (2005).
40. J. Vuckovic, M. Loncar, H. Mabuchi, and A. Scherer, "Optimization of the Q factor in photonic crystal microcavities," IEEE J. Quantum Electron. **38**, 850-856 (2002).
41. K. Srinivasan and O. Painter, "Momentum space design of high-Q photonic crystal optical cavities," Opt. Express **10**, 670-684 (2002).
42. J. L. Jewell, J. P. Harbison, A. Scherer, Y. H. Lee, and L. T. Florez, "Vertical-cavity surface-emitting lasers - design, growth, fabrication, characterization," IEEE J. Quantum Electron. **27**, 1332-1346 (1991).
43. J. P. Reithmaier, G. Sek, A. Loffler, C. Hofmann, S. Kuhn, S. Reitzenstein, L. V. Keldysh, V. D. Kulakovskii, T. L. Reinecke, and A. Forchel, "Strong coupling in a single quantum dot-semiconductor microcavity system," Nature **432**, 197-200 (2004).
44. S. Reitzenstein, C. Hofmann, A. Gorbunov, M. Strauss, S. H. Kwon, C. Schneider, A. Loffler, S. Hofling, M. Kamp, and A. Forchel, "AlAs/GaAs micropillar cavities with quality factors exceeding 150,000," Appl. Phys. Lett. **90**, 251109 (2007).

#100129 - $15.00 USD Received 13 Aug 2008; revised 18 Sep 2008; accepted 8 Oct 2008; published 15 Oct 2008

45. J. M. Gerard, B. Sermage, B. Gayral, B. Legrand, E. Costard, and V. Thierry-Mieg, "Enhanced spontaneous emission by quantum boxes in a monolithic optical microcavity," Phys. Rev. Lett. **81**, 1110-1113 (1998).
46. J. Vuckovic, M. Pelton, A. Scherer, and Y. Yamamoto, "Optimization of three-dimensional micropost microcavities for cavity quantum electrodynamics," Phys. Rev. A **66**, 023808 (2002).
47. L. Chen and E. Towe, "Photonic band gaps in nanowire superlattices," Appl. Phys. Lett. **87**, 10311 (2005).
48. O. Beyer, I. Nee, F. Havermeyer, and K. Buse, "Holographic recording of Bragg gratings for wavelength division multiplexing in doped and partially polymerized poly(methyl methacrylate)," Appl. Opt. **42**, 30-37 (2003).
49. E. M. Purcell, "Spontaneous emission probabilities at radio frequencies " Phys. Rev. **69**, 681-681 (1946).
50. T. Baba, "Photonic crystals and microdisk cavities based on GaInAsP-InP system," IEEE J. Quantum Electron. **3**, 808-830 (1997).
51. G. Khitrova, H. M. Gibbs, M. Kira, S. W. Koch, and A. Scherer, "Vacuum Rabi splitting in semiconductors," Nature Phys. **2**, 81-90 (2006).

1. Introduction

Semiconductor nanowires have recently emerged as novel light sources for integrated photonics. Lasers and electrically-driven light emitting diodes have been reported in various material systems (CdS, ZnO, GaN, etc) [1-5]. In all of these studies, a semiconductor nanowire is used both as the active medium and the Fabry-Perot optical cavity; the nanowire body serves as the optical waveguide, while its end facets serve as the mirrors bounding the optical cavity. However, due to the small diameter of a nanowire, significant evanescent field exists outside the nanowire body. This reduces the reflection of the nanowire facets and introduces significant losses, thus limiting the Quality factor, Q, of the cavity to ~500 [6-10]. In addition, the large evanescent field results in the small modal gain of the nanowire [11]. Both of these effects can increase the lasing threshold of nanowire lasers. At the same time, the Fabry-Perot nature of the optical cavity can result in multi-mode lasing, with lasing wavelengths dependent on the length of nanowire. In many applications single-wavelength emission with well-defined lasing wavelength is desired. The properties of nanowire lasers and LEDs could be improved by embedding nanowires into optical structures including photonic-crystals and race-track resonators [12], metallic gratings [13], and micro-stadium resonators [14]. However, to the best of our knowledge all previously reported structures based on nanowires had $Q \leq 1{,}000$.

In addition to their promise as low-threshold and high switching-speed nanolasers, semiconductor nanowires offer an attractive platform for the realization of electrically-injected, on-demand, single-photon sources. Solid-state version of single-photon sources based on self-assembled epitaxially-grown quantum dots (QDs) have been demonstrated in different microcavity configurations [15-17]. In all of these cases, a high Q and small mode volume (V_{mod}) of the microcavity were instrumental for achieving single-photon emission. Recently, there have been several proposals to achieve electrically-driven single-photon sources based on QDs embedded within semiconductor nanowires [18-25]. However, these reports did not consider the use of an optical cavity to improve the performance of such a source.

In this work, we propose an approach to significantly improve the Q of nanowire-based optical resonators, and we demonstrate cavities with $Q=3\times10^5$ and $V_{mod}<0.2(\lambda/n)^3$. Our approach is based on engineering a cavity in a one-dimensional (1D) photonic crystal (PhC) [12, 26] which is patterned around the nanowire. We demonstrate using numerical modeling that our platform coupled with a QD is well-suited for operation in the so-called strong-coupling limit of cavity quantum electrodynamics (QED), in which there is a coherent interaction between the photons confined to the optical nanowire cavity and excitons trapped in the QD [27].

#100129 - $15.00 USD Received 13 Aug 2008; revised 18 Sep 2008; accepted 8 Oct 2008; published 15 Oct 2008

2. Improvement of nanowire facet reflection using photonic crystals

In this work, we consider nanowires with a refractive index n_{wire}=2.8 and emission wavelength of λ≈500nm (e.g. CdS nanowires). However, our approach is general and applicable to different material systems. We assume a circular cross-section of our nanowires [Fig. 1(a)]. This allows us to take advantage of the radial symmetry of the system and significantly simplify the analysis. The more typical hexagonal cross-section of a nanowire is taken into account in the later section, and good agreement with our simplified model is found.

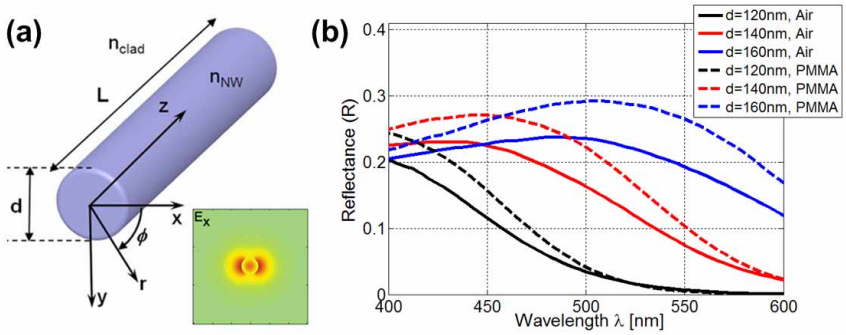

Fig. 1. (a) Schematic of nanowire and mode profile (E_x components) for fundamental HE_{11} mode with d=120nm and n_{clad}=1. (b) Reflectance of nanowire facets with air and PMMA cladding (HE_{11} mode).

First, we model nanowire as a cylindrical optical waveguide using Maxwell's equations in cylindrical coordinates [28, 29], considering the nanowire with air (n_{clad}=1) and low-index material cladding (e.g. polymer, n_{clad}=1.5). We find that nanowires with air (polymer) cladding support only the fundamental HE_{11} mode for d<150nm (d<160nm). This single-mode regime of operation is precisely the region that we are interested in for this work. Next, the reflectance of the nanowire facet was studied using the finite-difference time-domain (FDTD) method, and taking advantage of radial symmetry of the system. The fundamental HE_{11} nanowire mode is launched towards the nanowire end, and power reflected from the facet is monitored [Fig. 1(b)]. It can be seen that the nanowire facet reflectance is smaller than 25% (30%) for single-mode nanowires in air (polymer). Similar results have been found previously by other authors [7-9]. Such a poor facet reflection is responsible for large mirror losses and small quality factor (Q~500) of the optical cavity formed by the nanowire.

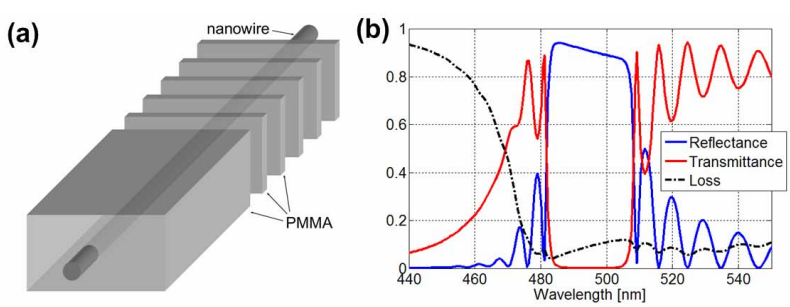

Fig. 2. (a) Schematic of a semiconductor nanowire with 1D PhC defined at its end. (b) Transmittance and reflectance spectra for nanowire with PhC consisting of 30 PMMA/air pairs.

In order to increase facet reflection and overall Q of the nanowire-cavity, we consider the structure shown in Fig. 2(a) [12]. The system consists of a nanowire embedded within polymer cladding, with 1D PhC defined at the nanowire end. One particularly appealing approach is to use Poly(methyl methacrylate) (PMMA) electron-beam lithography resist as the

#100129 - $15.00 USD Received 13 Aug 2008; revised 18 Sep 2008; accepted 8 Oct 2008; published 15 Oct 2008

cladding material. In this case, fabrication of the 1D PhC structure is very simple, and can be accomplished using electron-beam lithography, only.

In Fig. 2(b) we show the reflectance (R) and transmittance (T) spectra for the d=120nm nanowire with a grating of periodicity a=160nm. It can be seen that within the bandgap $\lambda \in$(486nm, 507nm), the reflectance can be as high as 95%, which is almost a 20-fold improvement over the facet reflection of bare nanowire. In Fig. 2(b) we also show the scattering loss, defined as L=1-R-T (absorption losses of the nanowire are neglected). This loss can be attributed to the scattering at the nanowire - 1D PhC interface, due to a mismatch between the propagating fundamental HE_{11} mode inside the nanowire and the evanescent Bloch mode that exists inside the grating section [30]. In the next section we will show that this scattering loss can be significantly minimized using techniques similar to the ones developed by Lalanne and colleagues [31, 32]. Outside the bandgap, at the short-wavelength (high-frequency) end, the loss increases significantly due to coupling to the leaky modes that exist inside the mirror section (the Bloch modes of the photonic crystal cross the light line and radiate energy).

It is important to mention that the position and width of the photonic bandgap will depend strongly on the nanowire diameter. Therefore, in an experimental realization of our platform, it is important that nanowires are straight and without significant diameter variations. Sophisticated growth techniques that result in straight and uniform nanowires have recently been demonstrated [10, 21, 23, 33, 34]. Finally, we note that photonic bandgap can close when the nanowire diameter is larger than 160nm, due to the presence of higher order modes.

3. Photonic crystal nanowire cavities

In this section we provide a detailed design of photonic crystal nanowire cavities taking advantage of the 1D PhC mirrors concept introduced in the previous section. We start with the Fabry-Perot cavity shown in Fig. 3(a) where the nanowire section of length s is sandwiched between two 1D PhC mirrors. We call such cavity *waveguide-mode* cavity. We select the same parameters used in Fig. 2(b) (d=120nm, a=160nm, 30 pairs of PMMA/air grating at each side), in order to assure single-mode behavior of the nanowire, as well as to position the emission wavelength of CdS (500nm) at the midgap of the PhC mirror. This provides the smallest penetration depth into the PhC mirror leading to a small mode volume, as well as minimizes the mirror transmission loss thus maximizing the overall Q. By tuning the cavity length (s), cavity modes with different symmetries can be formed and positioned precisely at the mid-gap frequency. The Q factors of these modes are 300, 395 and 500, for s/a=1.27, 1.95, 2.85, respectively. We note that it is possible to realize cavities with higher Q at the expense of an enlarged mode volume, by tuning the cavity resonance closer to the air-band edge. However, these modes are not of interest in this work due to the reduced Q/V_{mod} ratio.

The total Q factor of the 1D PhC cavity can be separated into transmission loss due to the finite length of the mirror, and the above-mentioned scattering:

$$\frac{1}{Q} = \frac{1}{Q_{sc}} + \frac{1}{Q_{tr}} \tag{1}$$

In our case, 30 layers of PhC mirror result in transmission quality factor of Q_{tr} ~10^5, which is significantly larger than the Q of *waveguide-mode* cavity obtained above. This implies that the dominant loss mechanism is scattering at mirror interfaces, as noted previously in Ref. [26]. In that work it was suggested that the mode profile mismatch between waveguide mode at the cavity region and Bloch mode is the main reason for large scattering losses. This mismatch can also be viewed as the effective index (effective impedance) mismatch between guided mode and the Bloch mode propagating in the mirror. From Fig. 3(c) we can see that the cavity guided mode has a mode index of n_{cavity}=1.72, while the evanescent Bloch mode positioned at the midgap frequency has a mode index of $n_{mid\text{-}gap}$=1.55.

#100129 - $15.00 USD Received 13 Aug 2008; revised 18 Sep 2008; accepted 8 Oct 2008; published 15 Oct 2008

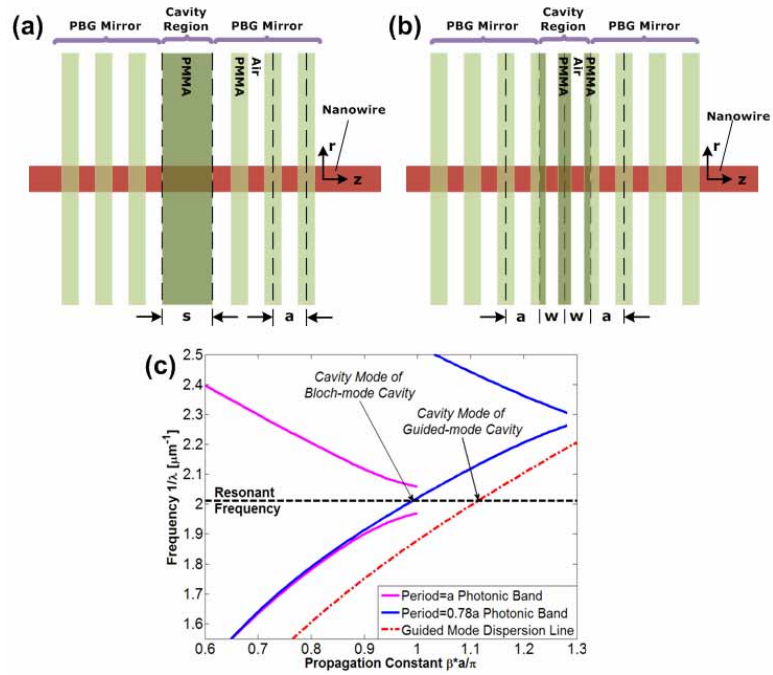

Fig. 3. (a) Schematic of *waveguide-mode* cavity. (b) Schematic of *Bloch-mode* cavity. (c) Dispersion line of Bloch mode with periodicity of 0.78*a* (blue), Bloch mode with periodicity of *a* (pink), and waveguide mode of nanowire embedded in PMMA (red).

To eliminate this index difference and the resulting mode mismatch, we substitute the uniform cavity region with a PMMA/air grating with the same duty cycle but a smaller period [Fig. 3(b)]. By choosing the period of this cavity section to be w=0.78a, we tune the cavity resonance to the mid-gap frequency of the mirror. Fig. 3(c) shows the photonic bands of the cavity segment as well as the PhC mirror. The propagating dielectric-band Bloch mode supported in the cavity region couples to the evanescent Bloch mode that exists within the bandgap of the PhC mirror to form the cavity mode. In contrast with the former design, the cavity mode here is a Bloch mode, and therefore the cavity is referred to as *Bloch-mode* cavity. The Q factor of our *Bloch-mode* cavity is 2,430 and the mode volume is $0.129(\lambda/n)^3$. As expected, the increase in Q is due to the reduced mode profile mismatch between the Bloch mode of the cavity and evanescent Bloch mode of the mirror. Recently another group have proposed similar cavity design in order to realize high-Q cavities [35].

Further Q enhancement can be realized by tapering the mode profile from the dielectric band to mid-bandgap by adding taper segments, as shown in Fig. 4(a). Two degrees of freedom are available to achieve the transition between the cavity Bloch mode and the evanescent Bloch mode of the mirror, namely the period (w) and the duty cycle of each segment. Here we keep the duty cycle fixed at 0.5, as we did in the cavity segment. Linear interpolation of grating constant ($2\pi/w$) of each segment is used to carry out the tapering process. Mid-bandgap resonance is achieved by altering the length of the central segment w_1. Similar tapering techniques were previously used to realize high-Q heterostructure cavities based on 2D PhC waveguides [36-38].

In Fig. 4(b) we present the dependence of the Quality factor on the number of segments placed in the taper region (one-segment structure corresponds to *Bloch-mode* cavity). For the case of 30 mirror pairs at each end (not including taper segments), Q first increases logarithmically as the number of taper segments increases, and then levels off when the number of tapers is larger than 5. When we increase the number of PhC mirror pairs to 40, the logarithmic dependence of Q on number of segments is recovered. Therefore, we conclude

#100129 - $15.00 USD Received 13 Aug 2008; revised 18 Sep 2008; accepted 8 Oct 2008; published 15 Oct 2008

that for large number of taper segments, transmission losses become dominant, and more mirror pairs are required. In Fig. 4(b), we also present the mode volume of the cavity calculated using Eq. (2).

$$V_{\mathrm{mod}} = \frac{\int_V \varepsilon(\vec{r})\left|\vec{E}(\vec{r})\right|^2 d^3\vec{r}}{\max[\varepsilon(\vec{r})\left|\vec{E}(\vec{r})\right|^2]} \tag{2}$$

As expected, the mode volume increases as the number of taper segments increases. However, the increase of V_{mod} is modest, especially for large number of taper segments. Moreover, in all cases the mode volume is smaller than $0.2(\lambda/n)^3$. This is due to the fact that we deliberately positioned the cavity mode precisely at the midgap frequency, and therefore the cavity field decays rapidly inside the PhC mirror. In the case shown in Fig. 4(c), Q/V_{mod} can be as high as 4.7×10^6 per cubic wavelength in material.

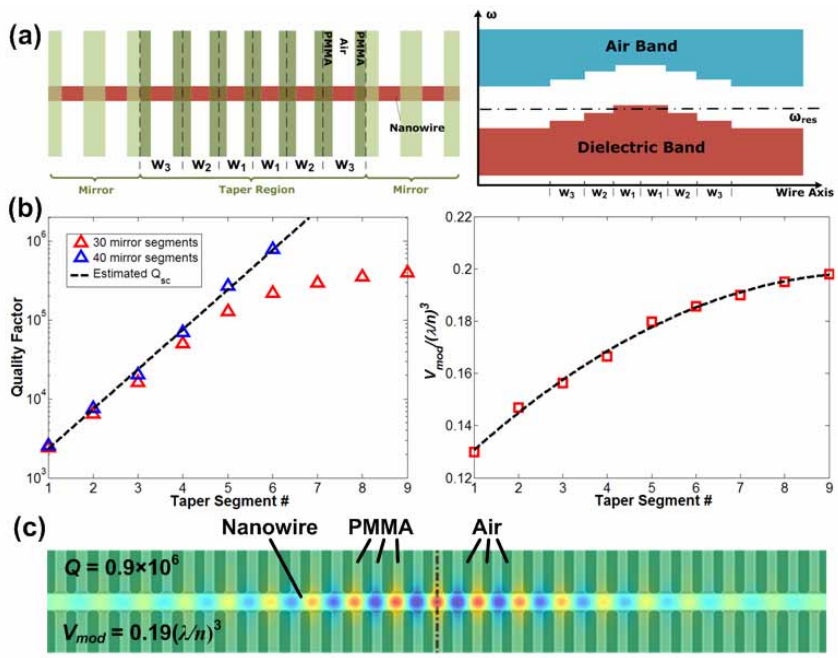

Fig. 4. (a) Schematic of photonic band tapering. (b) Quality factor and mode volume as a function of number of taper segments. In all cases, the cavity was designed to support one resonance positioned at the mid-gap wavelength of 497nm. (c) Mode profile of cavity modes (E_φ component) with 6 taper segments and 40 mirror pairs. Configuration of the tapered gratings is also mapped as background.

In previous paragraphs, we explained the ultra-high Q of our nanowire-based cavities using the mode-matching arguments. The high Q factor can also be explained by looking at the distribution of the cavity field energy in momentum space (k-space, spatial Fourier transform space) [17, 39-41]. In Fig. 5, we show the Fourier transform of the electric components E_φ of the cavity mode. $k_z=n_{clad}\omega/c_0$ defines the light line of the cladding. Components with k_z smaller than the light line support plane waves leaking energy radially into the cladding, and are responsible for scattering losses. The light cones in PMMA and air are colored in light green and dark green, respectively. We can see that as we include more taper segments, the Fourier spectrum of the mode profile concentrates more tightly around the edge of the Brillouin zone $k_z=\pi/a$, reducing the energy of the mode within the light cones, thus reducing the scattering. For comparison, the spatial spectrum of the *waveguide-mode* cavity,

#100129 - $15.00 USD Received 13 Aug 2008; revised 18 Sep 2008; accepted 8 Oct 2008; published 15 Oct 2008

shown in black, extends significantly inside the air and polymer light line, indicating large scattering losses.

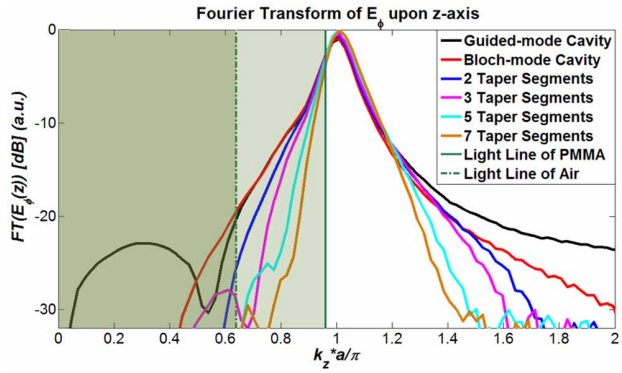

Fig. 5. Fourier transform of E_φ along wire axis. k-space zones within the light line are shown in green (light green within PMMA light line, dark green within air light line).

Our system is very similar to micropost (micropillar) optical microcavities that have been extensively used in vertical-cavity surface-emitting lasers [42] and single photon sources [15, 43-46], and more recently proposed in the context of semiconductor nanowires [47]. However, the big advantage of our approach that combines bottom-up synthesized nanowires with top-down fabricated photonic-crystals (only electron-beam lithography step), is simple fabrication procedure [12]. Complicated epitaxial growth of Bragg mirror, typical for conventional micropost cavities, is not required. Our technique is therefore fully compatible with different nanowire growth approaches including solution-based synthesis, vapor-solid-liquid, etc.

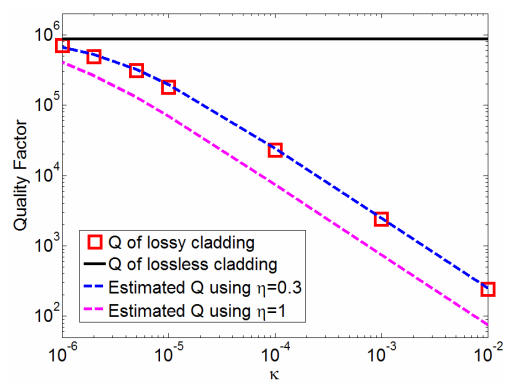

Fig. 6. Quality factor (red-square) as a function of imaginary part of refractive index (κ). The Q value with lossless cladding is indicated in black line. The dash lines represent estimation of Q using Eq. (3), while η=0.3 (blue) and 1 (magenta), respectively.

Next, in Fig. 6 we show how the overall quality factor depends on the material losses of the cladding (red-square), in the case of the optimized cavity (Q=0.9×10^6). Refractive index of the cladding is assumed to be of the form $n_{clad}+i\kappa_{clad}$, resulting in loss (1/Q) of the form $\eta\times 2\kappa_{clad}/n_{clad}$, where the coefficient η takes into account the overlap between the mode and lossy cladding (η <1). Thus the overall Q factor can be derived using Eq. (3).

$$\frac{1}{Q}=\frac{1}{Q_{lossless}}+\eta\frac{2\kappa_{clad}}{n_{clad}} \tag{3}$$

#100129 - $15.00 USD Received 13 Aug 2008; revised 18 Sep 2008; accepted 8 Oct 2008; published 15 Oct 2008

Using FDTD we found that η=0.3 (Fig. 6). In the case of PMMA cladding, κ_{clad} is smaller than 4×10^{-6} for wavelength of 500nm, that is the absorption coefficient of PMMA is smaller than α=0.1mm^{-1} [48]. As shown in Fig. 6, this loss results in small reduction of overall quality factor from $Q=9\times10^5$ to $Q=3\times10^5$. It is important to note that absorption coefficient of PMMA is even smaller (almost an order of magnitude) at red, near-infrared and telecom wavelengths (with the exception of two bands around 1100nm and 1400nm [48]) and therefore even higher quality factors can be obtained with nanowires emitting at these longer wavelengths.

Depending on the crystal structure of the nanowire material and the preferred growth direction, the nanowire cross-section can be triangular, square, hexagonal and so on. Here we consider nanowires with hexagonal cross-section embedded in our 1D PhC cavity [Fig. 7(a)]. First, the waveguide mode [Fig. 7(b)] and effective mode index of a nanowire with hexagonal cross-section is found. Next, the diameter of the equivalent cylindrical nanowire is chosen, so that it supports the mode with the same effective mode index. Then, a high-Q cavity is designed for the cylindrical nanowire by taking advantage of radial symmetry and using the optimization procedure described above. The same cavity design is then applied to the nanowire with hexagonal cross-section. In this way the optimization is done using 2D-FDTD with radial symmetry, which is significantly faster than performing a 3D-FDTD computation, which would be necessary for nanowires with hexagonal cross-section. Using this approach, we designed cavity for a nanowire with d_{hex}=130nm, using 40 mirror pairs and 5 taper segments. The resonance at λ=497nm had a $Q=9.4\times10^4$ and $V_{mod}=0.18(\lambda/n)^3$ [Fig. 7(c)]. Further optimization of the structure using 3D FDTD could result in even higher Q values.

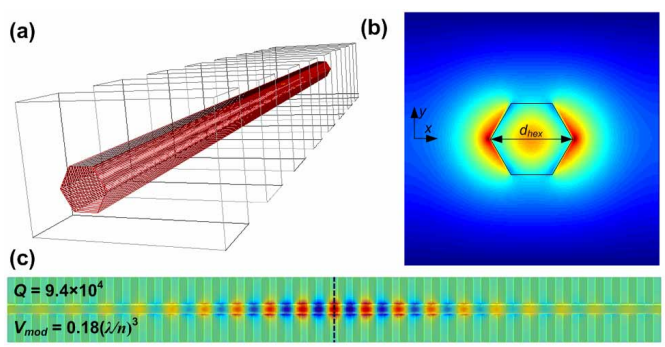

Fig. 7. (a) Schematic of hexagonal cross-section nanowire embedded in air/PMMA grating. (b) Mode profile of E_x component of hexagonal cross-section nanowire embedded in PMMA cladding. (c) Mode profile of cavity modes (E_x component) with 5 taper segments and 40 mirror pairs.

4. Light-matter interaction in semiconductor nanowire cavities

As first noted by Purcell [49], the emission rate of a radiating dipole can be modified by placing the dipole inside an optical cavity. The enhancement of the radiative emission rate into the cavity mode, when compared to the spontaneous emission rate without the cavity, can be described by the Purcell factor $F_0 = \frac{3Q\lambda^3\varepsilon_0}{4\pi^2 V\varepsilon_M}$ where V is mode volume of the cavity and ε_M is the dielectric constant at the field intensity maximum point. If F_0>>1, the dipole will emit much faster into the cavity than into free space. This increase in the radiative recombination rate is beneficial for the reduction of nanowire lasers threshold, and could result in the realization of threshold-less lasers [50]. In the case of a single-photon source based on a QD embedded within the semiconductor nanowire, the large Purcell factor means a high photon-production rate and a smaller probability for nonradiative recombination. Moreover, photons are preferentially emitted into the well-defined cavity modes and thus can easily be coupled out, using for example proximal optical waveguides, thereby increasing the overall collection

#100129 - $15.00 USD Received 13 Aug 2008; revised 18 Sep 2008; accepted 8 Oct 2008; published 15 Oct 2008

efficiency of generated photons. In our system we find that Purcell factor ($F=F_0/n_{wire}$) can be as high as 1.3×10^5 when 6-segment taper is used with material losses considered. It drops to 2.7×10^4 and 3.0×10^3 when four and two taper segments are used, respectively. Large Purcell factor is due to the ultra-high Q and very small V_{mod} in our cavity. The cavity may even enter the strong-coupling regime of light-matter interaction [27, 51], in which coherent exchange of energy between photon trapped in the cavity and exciton trapped in the QD exists. This happens when cavity field decay rate $\kappa=\omega/2Q$ and exciton decay rate γ (exciton loss due to the emission into non-cavity modes and non-radiative recombination channels) are smaller than exciton-photon coupling parameter g [46, 51]. For the cavity defined precisely around the quantum dot positioned in the center of the nanowire (at the electric field maximum), and transition dipole moment aligned with the electric field dipole, the coupling parameter can be expressed as $g=\Gamma\sqrt{V_0/4V}$ where g is the Rabi frequency of the system on resonance and $V_0=(3c_0\lambda^2\varepsilon_0)/(2\pi\Gamma\varepsilon_M)$. Here $\Gamma=n_{wire}\omega^3\mu^2/3\pi\varepsilon_0\hbar c^3$ is the spontaneous emission rate in the material. Assuming radiative life time of exciton without cavity to be 10ns, that is its radiative rate of Γ=0.1GHz we get coupling parameter g=190GHz. Typical values for non-radiative decay rates of excitons are bellow this value [51], and therefore the limiting factor for strong-coupling regime is cavity field decay rate. Therefore, we conclude that in our system, $g>\kappa, \gamma$ when $Q>10^4$ (κ<189GHz), and the system is well into the strong coupling regime even when only three taper segments are used.

Finally, we note that the most promising material systems used for realization of heterostructure QDs within nanowires are based on semiconductors with refractive index larger than $n_{wire}\approx2.8$ [23-25]. For example, in Ref. [24], the nanowire is based on GaP platform with n_{wire}=3.4. Our hybrid nanowire-1D PhC platform is general, and we confirmed that it can be used to realize cavities with high Q and small V_{mod} with these nanowires with larger refractive index.

5. Conclusion

Design of an ultra-high Q optical nanocavity consisting of a semiconductor nanowire embedded in 1D photonic crystal has been demonstrated. The mechanism of effectively suppressing cavity losses has been theoretically analyzed, and a cavity with $Q=3\times10^5$ and mode volume smaller than $0.2(\lambda/n)^3$ has been designed. Ultra-high Purcell factor, and operation in the strong-coupling regime are predicted in the proposed platform. High Q/V_{mod} cavities based on nanowires with hexagonal cross-section have also been designed. Our system is similar to micropost (micropillar) optical resonators that have been used in vertical-cavity surface-emitting lasers and single photon sources. However, our approach requires simple fabrication procedure that combines bottom-up nanowire synthesis with top-down single-step e-beam lithography.

Acknowledgments

Authors would like to acknowledge help by Murray W. McCutcheon. Yinan Zhang would also like to dedicate this work to Edgar Barroso and María del Rosario Hubert. This work was supported in part by NSF grant ECCS – 0708905 “NIRT: Photon and Plasmon Engineering in Active Optical Devices based on Synthesized Nanostructures” and by NSF Nanoscale Science and Engineering Center at Harvard University (http://www.nsec.harvard.edu/).

#100129 - $15.00 USD Received 13 Aug 2008; revised 18 Sep 2008; accepted 8 Oct 2008; published 15 Oct 2008